Influence of hydrostatic pressure and temperature on two-photon absorption of a C_{60}-2-thioxo-1,3-dithiole cycloadduct

B. Sahraoui,* I. V. Kityk,† and X. Nguyen Phu
Université d'Angers, Laboratoire des Proprietés Optiques des Matériaux et Applications, EP CNRS 130 2, Boulevard Lavoisier, Faculté des Sciences, 49045 Angers Cedex, France

P. Hudhomme and A. Gorgues
Laboratoire d'Ingénierie Moléculaire et Matériaux Organiques, UMR CNRS 6501, Université d'Angers 2, Boulevard Lavoisier, 49045 Angers Cedex, France

(Received 9 February 1998; revised manuscript received 30 September 1998)

Two-photon absorption (TPA) at $\lambda = 532$ nm versus applied hydrostatic pressure (p) (up to 20 GPa) and temperature (T) (in the 77–300 K range) was used to study intermolecular dynamics in powderlike fullerene-1,3-dithiolic adduct and C_{60} systems. For C_{60}-1,3-dithiole adduct, we observed a sharplike maxim of the TPA versus p-T below 230 K. Comparing the obtained results with those of C_{60}, we have unambiguously shown that the observed behaviors are connected with the adding of the 1,3-dithiole core. To explain the experimental results, we performed *ab initio* molecular-dynamics geometry optimization, taking into account the superposition of all possible molecular conformations with appropriate weighting factors and higher-order intermolecular multipole interactions. We have shown an increase of the absolute value of the TPA coefficient in the C_{60} cycloadduct by more than 30%. This fact is mainly caused by the asymmetry of intramolecular electronic charge-density asymmetry. The modulatedlike dependence of the TPA versus p and T have been observed. The latter one reflects the vibration and rotational contributions to the TPA values. [S0163-1829(99)07713-9]

I. INTRODUCTION

Chemical modifications of fullerenes have become very interesting from the viewpoint of improving their utility, stability, processibility, and optical nonlinearity.[1–3] However, producing modified C_{60} is a big problem due to difficulties in manufacturing an electron transfer added for enhancing their intermolecular interactions.[4,5] Still in view of achieving larger nonlinear optical susceptibilities many works were devoted to the synthesis of fullerenes by the adding of alkali metals.[6] Another very important aspect of the modification consists in the possibility of studying the contributions of electronic, vibration, and rotational subsystems to the observed nonlinear optical susceptibilities.

Recently the fullerene derivatives have been widely studied for their third-order nonlinear optical properties and they effectively showed very large third-order nonlinear optical properties.[7,8] To achieve an increase of the nonlinear optical susceptibility coefficient one should enhance intermolecular interaction and intramolecular noncentrosymmetric charge-density distribution. It is well known that the fullerene molecules preserve a strong individuality. In Ref. 9 it was shown how to bring an essential contribution of frozen-in orientation disorder of the C_{60} molecule to the measured dielectric susceptibilities. Therefore, one can expect the same contribution to the higher-order nonlinear optical susceptibilities. The intermolecular overlap leads to an increase of π-electron delocalization, which favors an increase of the intramolecular hyperpolarizability. To reach a high intermolecular interaction and high nonlinear optical hyperpolarizability of the C_{60} molecule, we have grafted the 2-thioxo-1,3-dithiole moiety. This should lead to additional intermolecular overlaps.

The effective tools for continuously changing the intermolecular interaction, molecular mobility, and intramolecular charge transfer, were external hydrostatic pressure and temperature. During our consideration besides the pure electronic contribution to the nonlinear optical susceptibility we took into account also the vibration and rotational contributions. The high mobility of the investigated molecules afforded some ambiguity in describing the molecular dynamics (i.e., dynamics boundary conditions vary so fast in time that the differential equations became very difficult to solve). To overcome this complication, we used the static approach which is based on a superposition of separate molecular conformations for a given moment of time, which is renormalized by appropriate Boltzmann weighting factors.[10] At the same time it was very important to consider intermolecular multiple interactions of higher orders.[11] On the other hand, only appropriate quantum chemical molecular-orbital (MO) calculations with the inclusion of excited configuration interaction (CI) states gave complete information about quantitative nonlinear optical susceptibilities in the C_{60}-1,3-dithiole adduct. Therefore, we replaced time-dependent Hartree-Fock procedure[12] by a time-averaged (static) molecular structure. Recently this static approach has been successfully applied to study the third-order optical properties of some tetrathiafulvalene derivatives.[11] The reason why this method works, can be easily understood if we think about the role played by statistic molecular interaction and the vibration-rotational interactions in optical response of the investigated compound.[13,14] The main aim of the present work consists in the investigation of the external-induced changes in modified fullerenes in order to detect the changes of intermolecular electronic kinetics using optical methods.

The paper is organized as follows: the experimental methods are described in Sec. II. In Sec. III we present the observed p-T dependences of the TPA. Molecular dynamics and geometry optimization procedures are presented in Sec.

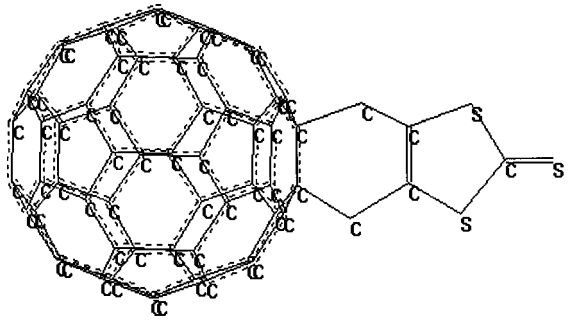

FIG. 1. Scheme of the modified fullerence: C_{60} and 2-thioxo-1,3-dithiolie cycloadduct 1.

IV. Section V is devoted to electronic charge-density distribution calculations. The influence of the electron-vibration-rotational (EVR) interactions on the TPA parameters is presented in Sec. VI.

II. EXPERIMENTAL TECHNIQUE

The chemical formula of the C_{60}-2-thioxo-1,3-dithiole cycloadduct is presented in Fig. 1. The technology of producing this compound is described in Ref. 15. We shall only briefly describe the synthesis of this mentioned compound in this paragraph. The cycloadduct 2-thioxo-1,3-dithiole was synthesized using the Diels-Alder reaction[16–18] between the 2-oxo-4,5bis (methylene)-1,3-dithiole and C_{60}. This diene was generated by the thermal rearrangement of the *S*-propargyl xanthate. This last compound (292 mg, 1.04 mml) was heated for 2 h in dry chlorobenzene (400 mL) in the presence of 1.035 g (1.44 mol) of C_{60} under a nitrogen atmosphere. After silica gel column chromatography (CS_2 then toluene as eluents), the mono, bis, and trisadducts were separated, respectively, in 60, 5–10 %, and below 5% yields. The basic cleavage of this 2-oxo-1,3-dithiole adduct was achieved by treatment with a sodium methoxide solution. Then the disodium dithiolate was trapped by thiophogene leading to the C_{60}-2-thioxo-1,3-dithiolie compound in a 65% yield.

The synthesized samples had a powderlike form with diameter sizes lying within the 10–20 μm range. The powderlike specimens were dissolved in liquid oligoetheracrylate photopolymer matrices. The solidification process and electropoling homogenization have been carried out using a method described in the Ref. 19. A nitrogen laser ($\lambda = 337$ nm) with the photon energy power about 45 W/cm^2 was used for the solidification. This equipment allows us continuously to vary specimen thickness within the 0.5–1.2 cm range with a step of 0.1 mm. Homogenization procedures have been carried out using ultrasound mixing and crushing and control of the specimen homogeneity has been carried out using the optical polarized method. We have revealed that the deviation from the homogeneity was less than 3.2% through the specimen surface and higher homogeneity was obtained for the cycloadduct concentration about 2.3 at. wt%.

The excitation was provided by picosecond pulses of $\lambda = 1.06\,\mu$m and $\lambda = 530$ nm generated by a YAG:Nd laser. The laser light was polarized using a rotating Fresnel polarizer and the output light intensities was detected using a FEU-79 (FEU-39) photomultipliers. The measurements were carried out in the single-pulse regime, with a pulse frequency repetition of 12 Hz and the tunable pulse duration within the 0.6–50 ps. Such short-time kinetics allow us to avoid the specimen heating. The pumping laser beams have been scanned through the specimen surface in order to avoid the specimen nonhomogeneity contributions. The measurements have been carried out both for the transmitted beam as well as for the scattered light beams. Therefore for every thickness we have obtained more than 120 measured points for the penetrated *T*, reflected and scattered *R* light intensities. Laser power beams have been diagramed to obtain the light profile inhomogeneity (usually of the gaussian form) not less than 95% of the maximum light intensity for the energy powers within the $0.75\times - 1.1$ GWt/cm^2 range. Measurements devices both for the transparent and reflected channel have been synchronized. Developing the expression $T \approx 1 - \beta l I_p$, where β is the two-photon absorption coefficient, l is the thickness of investigated sample (0.5 mm), and T is the intensity-dependent transparency for the case of the intensity-dependent scattered and reflected light with total coefficient *R*, we have calculated the absorption coefficient according to the formula: $K(I) = 1/d \ln\{(1-R(I))/2T(I) + [(1-R(I))^2/4R(I)^2]\}$. Evaluating the dependence of the *K* versus the *I*, we have extracted the two-photon absorption coefficient β. Statistical treatment using the χ^2 Student approach gives us a reliability with an error margin not larger than 0.03. Due to the close values of refractive indices for the oligoetheracrylate matrices and the fullerenelike specimens, the light background scattering did not exceed 7%.

To calibrate absolute values of the output intensity, the LiB_3O_5 nanoparticles embedded in the oligoetheracrylate matrices were used. Independently, we performed measurements for the samples of C_{60} and for the proper oligoether matrices. The last one was necessary in order to eliminate an influence of photopolymer matrix background. The TPA signal was extracted from the intensity-dependent transparency measurements. Simultaneously we have extracted the influence of linear absorption (220 cm^{-1}, $\lambda = 530$ nm) and the influence of Fresnel reflection 0.048. The choice of the oligoetheracrylate matrices is caused by the low value of their TPA coefficient (below 0.002 cm/GW) and close values of the corresponding refractive indices. The averaging statistics over the sample surface was performed to avoid a space nonuniformity in the sample distribution within the photopolymer oligoetheracrylate matrices.

To exclude an influence of the hyper-Raman scattering, we have performed additional investigations of the scattered light from the wavelength $\lambda = 530$ nm up to 3000 cm^{-1}. We have detected three hyper-Raman maxima between 1200 and 1800 cm^{-1}. Their intensities were at least 13 times weaker than the transmitted light intensity. In the case of the Raman and hyper-Raman measurements, we have used an argon (Ar^+) laser at the 522 nm line and a Spex Triplemate spectrometer. A position-sensitive photomultiplier calibrated using a helium-neon gaseous mixture discharge was used to detect the integrated scattering background.

For optical measurements under applied hydrostatic pressures, we have constructed a special thermo-baro chamber with sapphire windows which allowed us to perform the corresponding measurements in high-pressure atmosphere within the temperature range 77–450 K. A Mao-Bell-type

diamond-anvil cell supplied with diamond optical windows was used for measurements. The pressure and the temperature were changed within the 0.1–20 GPa and 77–450 K regions, respectively. The precision of the pressure and temperature stabilization were equal to ± 0.2 GPa and to ± 1 K, respectively. All the measured optical parameters were averaged over a great number of pulses (about 120–150) for each p-T point. Afterwards, we have performed a fitting procedure using a spline smoothing and χ^2 statistics with a parameter not more than 0.02.

We have used a mixture of 15:5:2 methanol:ethanol:liquid nitrogen or liquid argon as the pressure medium. Ruby fluorescence was used for hydrostatic-pressure determination of pressure gradients. Our apparatus allows us to perform the TPA registration in the transparent geometry (parallel spreading of the pumping and probing beams). The intensity of the laser beams was varied using neutral density filters. A time-delay between the pump and tunable probe pulse was obtained using the $Li_2B_4O_7$ single crystal. The reliability of the obtained results lies within 35%.

III. EXPERIMENTAL RESULTS

In Fig. 2 we present the measured pressure-temperature (p-T) dependences of the TPA for the C_{60} and C_{60}-1,3-dithiole compounds. One can see a modulation of the TPA versus p and T at temperature below 235 K for the modified C_{60}. We should notice that for temperatures below 190 K the p-T TPA dependences are sharper compared with the higher temperatures. In the case of C_{60}, only one wide maximum for temperatures higher than 250 K is observed, which is probably connected with the temperature-orientation disordering. We performed also measurements for benzene alcohol and benzene toluene solutions at room temperature in order to estimate an influence of solvent on the final TPA coefficients. We revealed that solvents did not influence significantly the estimations of the nonlinear optical susceptibilities. The only problems consists in their higher scattering coefficients.

The observed data did not show any pressure-temperature hysteresis. The relative modulation of the TPA versus p-T did not exceed 35%. The estimated values of the TPA coefficient β for C_{60} and C_{60}-2-thioxo-1,3-dithiole adduct are presented in Table I. We observe that the grafting of the 1,3-dithiole core induces an increase of TPA. We notice also that the β values are slightly dependent upon the environment of the investigated samples.

Moreover, in the case of the modified C_{60} compound, we observed a slight increase of the TPA with increasing pressure contrary to the case of C_{60} (Fig. 2). At lowering temperature C_{60} showed a smooth decrease of the TPA. In the case of modified C_{60}, we observed a sharp maxima with half-widths of 45 K and 0.8 GPa. The observed phenomena are clearly caused by the linking of the 1,3-dithiole core. The curve of the TPA versus p-T indicates the important role played by the 2-thioxo-1,3dithiole fragment in the illustrated experimental results. In the case of C_{60} we have only one maximum increasing with the pressure. The observed maxima for C_{60} and C_{60}-1,3-dithiole demonstrated a sensitivity to intermolecular interactions of the TPA method.

TABLE I. Comparison of the two-photon absorption coefficient β, obtained using different theoretical approaches and experimental methods. β is the theoretical value for C_{60} and C_{60}-cycloadduct without inclusion of the electron-vibration-rotation interactions, $\beta^{(1)}$ is the theoretical value for C_{60} and C_{60}-cycloadduct with the inclusion of electron-vibration-rotation interactions, $\beta^{(2)}$ is the experimental value for C_{60} and C_{60}-cycloadduct embedded in the oligoetheracrylat matrices, $\beta^{(3)}$ is the experimental value for C_{60} and C_{60}-cycloadduct in benzene alcohol solution, and $\beta^{(4)}$ is the experimental value for C_{60} and C_{60}-cycloadduct in benzene-toluene solution.

Sample	β (cm/GW)	$\beta^{(1)}$ (cm/GW)	$\beta^{(2)}$ (cm/GW)	$\beta^{(3)}$ (cm/GW)	$\beta^{(4)}$ (cm/GW)
C_{60}	12.7	15.6	18.6	18.5	18.75
C_{60} cycloadduct	14.8	23.5	26.7	26.45	27.35

IV. MOLECULAR DYNAMICS

To optimize the molecular geometry, we started from the isolated molecule using the MM^+ method and derivative procedure of Broyden-Fletcher-Goldfarb-Shanoo[20–24] with variable effective clusters cutoffs. Their radius was varied from 14 to 29 nm with increments of 0.5 nm. The convergence was achieved when the difference between the two successive values of the optimized total energy is less than 0.02 Ry. Then we introduced the effective intermolecular multipole interactions of higher order (and quadrupole-quadrupole interactions). These higher interactions are especially important for the disordered materials.[25] We built up the structural clusters taking into account different values of

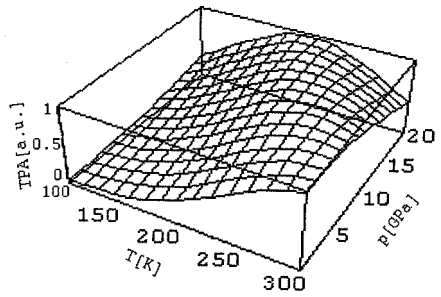

(a)

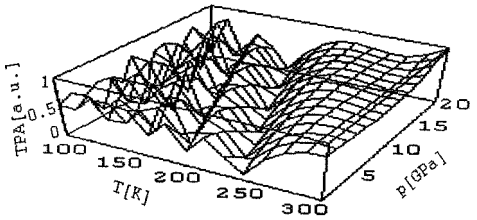

(b)

FIG. 2. Pressure-temperature dependence of the TPA in (a) C_{60}, (b) C_{60}-1,3-dithiole. All the measurements are carried out for the 0.53 μm wavelength.

the optimized total potential energy. We performed a self-consistent iteration procedure with continuously (step-by-step) increasing values of the total energies for a given molecule. To introduce values of the partial contributions of the given conformation and applied pressure, we renormalized this procedure using appropriate weighting factors proportionalllly to their probability p_i for a given phase:[10]

$$p_i = \exp(-U_i/k_BT)/\Sigma \exp(-U_j/k_BT_j), \tag{1}$$

where U_j represents total energy minimized at temperature T_j and k_B is the Boltzmann constant.

We began the optimization using a self-consistent iteration procedure from low temperatures, i.e., 0.5 up to 210 K. Then we applied the hybrid Becke's methods[26] involving a semiempirical contribution of the ''exact'' exchange E_x^{HF} (i.e., Hartree-Fock type, but based on Kohn-Sham orbitals) and the exchange energy E_g^{LSDA} (LSDA means the local-spin-density approximation) in the density-functional theory (DFT), together with a gradient-corrected correlation functional E_C^{LSDA}. The total DFT calculations have been performed using a GAUSSIAN-94 program[27] using the polarized correlation consistent double ζ basis sets (cc-pVDZ).[28] The main advantage of the mentioned method consists of very fast convergence with respect to the size of the basis sets. But more important was the possibility of introducing an external scalar perturbation such as pressure in order to predict the pressure-dependent geometry optimization because we are able to vary the inter- and intramolecular distances proportionally to the second space derivative of the electrostatic potential. The improved integral grid[29] (option FINEGRID) and tight criteria were used in the self-consistent functional calculations.

The optimized modified C_{60} compound under applied pressure and without the applied pressure are given in Fig. 3. It seems that the more interesting observations are the bends of the 1,3-dithiole plane under the applied pressure. It gives a rise to additional rotating axes shifted towards the fullerene rotation axes. This fact can play an important role in intermolecular interactions.

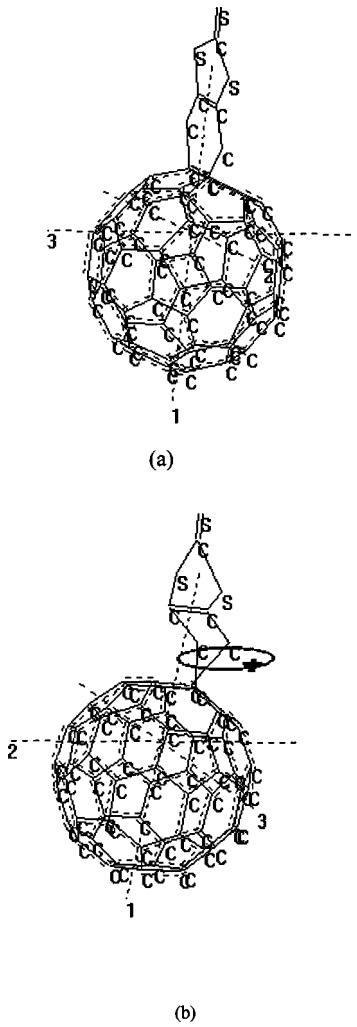

FIG. 3. Perspective view of the C_{60}-1,3dithiole molecule without (a) and under (b) applied pressure. By arrows we indicate main direction of C_{60}-1,3dithiole rotation direction and their orientation relative fullerene axis.

V. MOLECULAR ORBITAL QUANTUM CHEMICAL CALCULATIONS

We performed the molecular orbital calculations using tight-binding method and linear combinations of atomic orbital (LCAO) centered at neighboring atoms.[30] To avoid an influence of boundary conditions, the effective macroscopic dielectric susceptibility was introduced to renormalize the intramolecular energy levels. We introduced an effective quasiwave vector **k**, corresponding to the sizes of the molecular-dynamics geometry optimized molecules.

The tight-binding quasiwave functions can be expressed using the quasi-Bloch theorem in the case of a real-space representation:

$$\chi_{\mathbf{k},n}(\mathbf{r}) = N^{-1/2} \sum_{\tau} \exp(i\mathbf{k}\tau_n) |1, \mathbf{r} - \tau_n\rangle \tag{2}$$

where $|l\rangle$ is the orbital of l-orbital angular momentum symmetry (i.e., s, p, d, etc.) and τ_n is the position vector of nth atom. The one-electron quasiwave function of the molecule is usually written as a linear combination of the above basis quasiwave functions within a momentum representation:

$$|\mathbf{k}\rangle = \sum_n C_n |\mathbf{k}, n\rangle \langle \chi_{\mathbf{k},q} | \hat{H} - E(\mathbf{k}) | \chi_{\mathbf{k},q'} \rangle \sum_q \exp(-i\mathbf{k}\tau_q)^*, \tag{3}$$

which is often called the Bloch sum; $\chi_{k,q}$ are weighting factors of the corresponding quasiwave vectors; $E(\mathbf{k})$ is the eigenvalue at the **k**th quasiwave vector. Summation limits are very important since they determine the cluster sizes and the number of the coordination spheres around the considered molecule.

It seems interesting to use the self-consistent method of linear tetrahedra for the calculation based on the so-called restricted model.[31] Thus the traditional overlapping-atomic-potential approach for the one-electron Hamiltonian was calculated as a superposition of individual free-atom potentials (with the Slater-type approximation for exchange integrals) at appropriate positions. All the Hamiltonian matrix elements were computed using the Gaussian technique for Bloch sums of the atomic orbitals as basis functions. At this step we have included the unoccupied molecular orbital states of the

norm-conserving pseudopotential functions obtained from pseudopotential (PP) methods[32] which were corrected by the LCAO procedure (by the orthogonalization of the intramolecular terms) in order to obtain the best agreement with the experimental energy gap. Therefore in each step we construct the superpositions of the starting basis coming out from the appropriate superposition of the PP and LCAO quasiwave functions with the corresponding weighting factors. In such a way we combined the advantages of the two methods.

The core states were removed from the basis set to restrict the maximum size of the secular equation set. The remaining occupied orbitals were simultaneously orthogonalized with respect to the core states. Such a scheme of the orthogonalization allowed us to restrict the Hamiltonian diagonalization to a matrix size of 866. The basis set size has been afterwards increased up to 1685 with the energy cutoff up to 236 Ry. A main iteration criterion to ensure an eigenstate stabilization consists of a coincidence of two neighboring energy eigenvalues within a range of 0.01 Ry.

True orbitals of free atoms were replaced by local functions of the Slater type which are very similar to the true first-principles atomic quasiwave functions, although the former take part in a distortion of the electron distribution. A set of the optimized orbitals obtained in such a way can be numerically estimated by a technique of the constructed Gaussians described in Ref. 33. We have built the orthogonalized Bloch sums in the following form:

$$\mathbf{B}_{q'\alpha}(\mathbf{k},\mathbf{r})=B_{q\alpha}(\mathbf{k},\mathbf{r})+\sum_{y=1}^{N}\sum_{l=0}^{N_\infty} a_{q\alpha,1\gamma}\mathbf{B}_{1\gamma}(\mathbf{k},\mathbf{r}), \quad (4)$$

where the $B_{1\gamma}(\mathbf{k},\mathbf{r})$ expression is restricted to the unoccupied MO obtained from PP quasiwaves. All $\alpha_{q\alpha,1\gamma}$ and $B_{1\gamma}$ coefficients are calculated with regard to the orthogonality conditions of the previously calculated norm-conserving PP quasiwave functions.

A potential of the one-electron Hamiltonian was constructed as a superposition of the atomiclike potentials $V_\alpha(r)$. The atomic potentials were approximated by the following expression:

$$V_\alpha(\mathbf{r})=(-Z_v e/r)\sum_{i=1}^{n'}[c_i\exp(-\alpha_i r^2)+A_i r^2\exp(-\beta_i r^2)], \quad (5)$$

where all the fitting coefficients c_i, α_i, A_i, and β_i were calculated using a nonlinear interpolation scheme.[34] The set of 8–12 Gaussians was used to provide a good fit of the radial functions in our calculations. All the Hamiltonian matrix elements were decomposed into a series of three-center integrals containing two Gaussians centered at the local atomic positions **A** and **B** and the atomic potential around the point **C**.

The matrix elements were expanded by using a special point summation method of multicenter integrals. All the summations were carried out by solving the set of equations:

$$\{H_{ij}(\mathbf{k})-E(\mathbf{k})S_{ij}\}=0, \quad (6)$$

for various points within the effective molecule. It was necessary to calculate the matrix element values with much higher precision than a desired accuracy of the eigenvalues due to the large size of the obtained set from secular equation (6). The summations were performed up to eight neighbors. We performed the numerical integration in a real space approximation to take into account a contribution of electron-electron interactions (the so-called Hartree functional). An example of the overlap integrals for *s*-wave and *p*-wave states were determined by the following formula:

$$\langle s_a|s_b\rangle=\frac{1}{4\pi}\sum_{i=1}^{N}\sum_{j=1}^{k} c_i c_j[\pi/(\alpha_i+\beta_j)]^{3/2} \times\exp\{[-\alpha_i\beta_j/(\alpha_i+\beta_j)](\mathbf{B}-\mathbf{A})^2\}, \quad (7)$$

$$\langle s_a|p_{xb}\rangle=\frac{\sqrt{3}}{4\pi}\sum_{i}\sum_{j} c_i c_j\{[\pi/(\alpha_i+\beta_j)](\mathbf{B}-\mathbf{A})^2\} \times\exp\{[-\alpha_i\beta_j/(\alpha_i+\beta_j)](\mathbf{B}-\mathbf{A})^2\}DB_x. \quad (8)$$

The matrix elements of the Hartree-Fock operator are

$$F_{ij}=c_i c_j[\pi/(\alpha_i+\beta_j)]^{3/2}\exp\{[-\alpha_i\beta_j/(\alpha_i+\beta_j)](\mathbf{B}-\mathbf{A})^2\}. \quad (9)$$

The position **D** of the mass center of the **A** and **B** atoms can be written in the following way:

$$\mathbf{D}=(\alpha_i\mathbf{A}+\beta_j\mathbf{B})/(\alpha_i+\beta_j), \quad (10)$$

with $DB_x=D_x-B_x$ and $DA_x=D_x-A_x$. The other overlap expressions used in our calculations have been presented before.[31] Electron screening effects were calculated using parametrized Perdew-Zunger[35] and Ceperley-Alder expressions[36] of the following form:

$$\mu_{xc}=-0.6193/r_S-0.14392/(1+1.0529{r_S}^{1/2}+0.3334r_S) \times\{1+[(0.5264{r_S}^{1/2}+0.3334r_S)/(3(1+1.0529{r_S}^{1/2} +0.3334r_S))]\} \quad \text{for } r_S>1 \quad (11)$$

$$\mu_{xc}=-0.6193/r_S+0.031\ln(r_S)-0.0583 \quad \text{for } r_S<1, \quad (11a)$$

where $r_S=[3/(4\pi\rho)]^{1/3}$ with ρ being the electron density and the first terms of Eq. (11) and Eq. (11a) correspond to the standard Gaspar-Kohn-Sham exchange potential.

A special point method of Chadhi-Cohen[37] was used for the intramolecular summation of the electron charge-density distribution. This last was used to construct a charge-density functional for electrons. The diagonalization procedure was performed at special symmetrical weighting points of the molecule.

The needed self-consistency was achieved by a direct iteration process. Acceleration of the iteration convergence was achieved by mixing the $(m-1)$th iteration with 80% of the output ρ before their substitution into the next equation. The initial screened potential has been built using the Thomas-Fermi approximation which avoids possible errors during the electron density calculation. A criterion of the self-consistency in the charge-density formalism requires that

$$|\rho_{\text{out},m}-\rho_{\text{in},m}|<\varepsilon \quad (12)$$

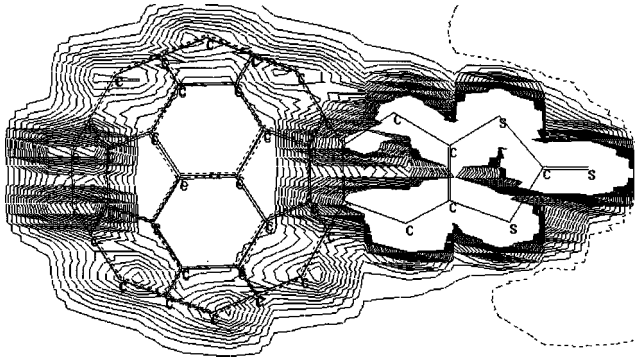

FIG. 4. Charge-density distribution in the modified C_{60} molecule.

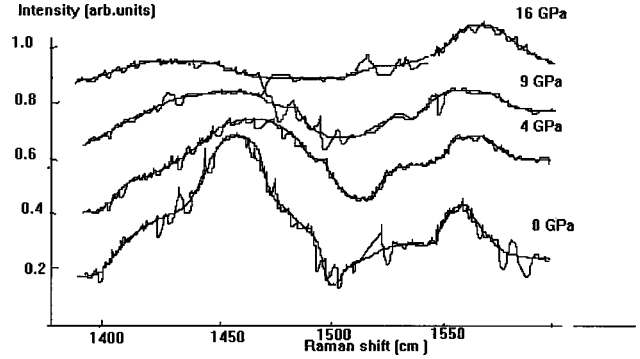

FIG. 5. Change of the Raman spectra fragment under the applied pressure.

after the mth iteration step, we assumed an accuracy better than $\varepsilon = 0.10\%$ between the input and output iterations as a main criterion of the self-consistency. The energy eigenvalues were stable within a range of 0.005 energy atomic units. The procedure of Hermitian diagonalization was performed using the Querry limited method.[38]

The Hamiltonian has been diagonalized at 124 equally spaced points in the 1/64th part of the molecule in order to enhance a description precision of the electronic density of states. The numerical evaluations were performed using a tetrahedral method. The more detailed expressions for overlap integrals can be found in Ref. 31.

In Fig. 4 we present the results of MO electronic charge-density distribution calculations for the isolated modified C_{60} molecule using the described above method. From the Fig. 4 one can clearly see an essential redistribution of the charge-density distribution near the 1,3-dithiole core. Moreover, directly on the border between C_{60} and the dithiolic moiety, one can see essential intramolecular charge-density redistribution and several asymmetries. The last fact supports our previous prediction about the essential role of the charge-transfer noncentrosymmetry in the molecule. It is necessary to add that the contributions to the total charge-density distributions give both the intra- and intermolecular interactions. As a consequence, we noted an accentricity both in the fullerene sphere as well in the edges of the 1,3-dithiole core. So we can speak about the combined effect of the intramolecular and intermolecular charge-density asymmetry. The presented charge-density distribution helps also in clarifying the contributions to the Hessian matrices determining the quasiphonon harmonics contributions. Our calculations indicate the essential role of the intermolecular interacting component in the prediction of the nonlinear optical susceptibility. Moreover, the mentioned charge-density redistribution shows the necessity of considering also the corresponding electron-vibration and electron-rotational contributions to the output susceptibilities. The quantitative results are presented in Table I.

VI. ELECTRON-VIBRATIONAL AND ROTATIONAL CONTRIBUTIONS

In order to get a good agreement between the observed behavior of the TPA versus p-T and the quantum chemical model we included the contributions of vibration and rotational subsystems into dipole moments.

In our previous works[39–41] we have shown the possibility of detecting the electron-vibration anharmonicity in high-temperature superconducting single crystals by nonlinear optics methods. The corresponding behaviors seem to be very close to the low-temperature detection of the electron-vibration rearrangement of the system, but in the case of fullerenelike compounds we preferred to classify the behavior as a low-temperature structural rearrangement that leads to partial long-range ordering. In the case of fullerenes such methods can be useful for the interpretation of the temperature-orientational reordering.

This method was successfully applied by us to investigate the electron-vibration contribution to the nonlinear optical susceptibility of tetrathiafulvalenes[10] and chalcogenide glasses.[25]

The obtained data in this work suggest that the above theoretical approach can help to clarify the origin of molecular orientations and problems of the critical temperature increase. Simultaneously it was necessary to stress that the observed phenomena can be explained by low mobility of free carriers due to their self-localization in disordered traps sublevels. The quantum chemical calculations were performed self-consistently after separation of the electronic, vibration, and rotational degrees of freedom. Therefore, in order to decrease a number of active Raman modes and to include in the quantum chemical considerations only the modes sensitive to the intermolecular interactions changing under the applied pressure, we performed measurements of the Raman spectra. Here we should distinguish two types of sensitive modes. The first one corresponds to the intraplain cycloadduct vibrations and are sensitive to the bending of the plains. The second one is responsible for the changes of the intracycloadduct bond lengths. As a consequence the first type of mode should vanish with increasing hydrostatic pressure and the second one should change the frequency. In Fig. 5 are presented the modes corresponding to the first type of vibration. One can clearly see their sensitivity to the disappearance of the cycloadduct plains. Moreover, one can see an essential damping of the modes due to their widening. On the other hand, in Fig. 6 are presented modes that are sensitive to the changes of the intracycloadduct bond distances. The latter ones reflect only a shift of the distances within the cycloadduct group. From Fig. 6 one can clearly see that the modes sensitive to the bond distances under the applied features possess higher frequencies in accordance with our estimations and for both types of modes an abrupt change is

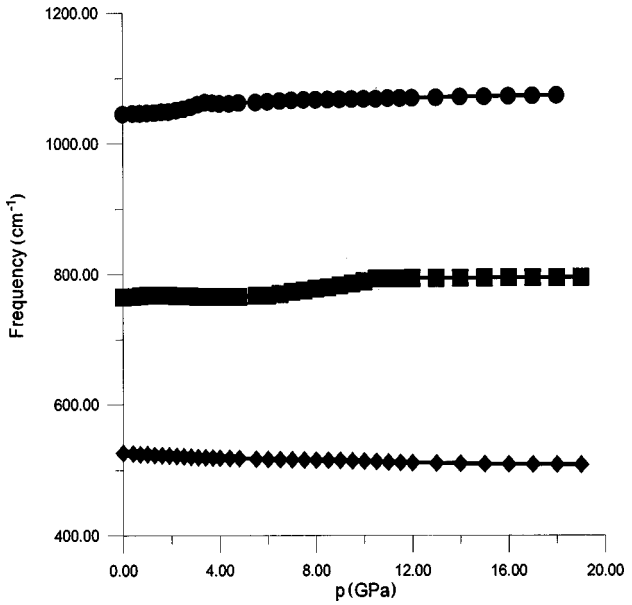

FIG. 6. Pressure dependence of the three Raman modes which are more sensitive to the intermolecular interaction.

observed for pressures about 7.8 GPa. We present only the modes more sensitive to the applied pressure.

The more important observation is the independence of the observed Raman spectra of the external solvents, particularly from benzene-alcohol and toluene-benzene solution compared with the data obtained for the powder embedded within the oligoetheracrylate matrices. As a consequence, we note the possibility of using the solidified photopolymer oligoetheracrylate matrices for the mentioned sample.

Contributions of a particular vibration mode to the output nonlinear susceptibility takes place through an electron-vibration interaction, particularly with the excited configuration interaction (CI) states. An example of such a CI-vibration mode (at 1027 cm^{-1}) is shown in Fig. 7. These kinds of electron-vibration functions modulated by a rotational wave function give an essential additional contribution to the total TPA coefficients. Particularly, the mentioned mode gives the contribution within 15–22 %.

To consider the contribution of the vibration subsystem we use the method of the Green function in a standard

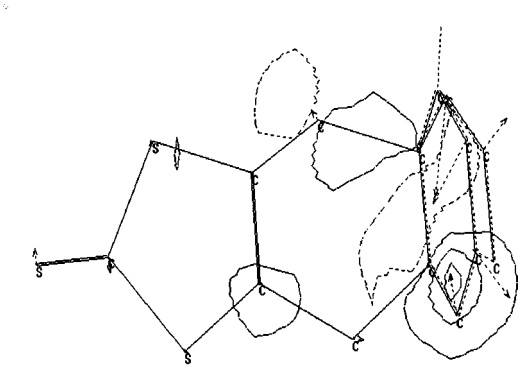

FIG. 7. The typical electron-vibrational fragments contributing effectively to the final nonlinear optical susceptibility.

approximation.[40] The Green functions were calculated by summations over 864 points within the effective molecule. The influence of neighboring molecules was taking into account by consideration of the effective local Lorentz field renormalized by the appropriate eigenvalues and eigenvectors. The quantum chemical calculations were performed self-consistently after separation of the electron and vibration degrees of freedom. Schrodinger equation for a purely vibration motion may be expressed in a harmonic approximation:[41]

$$d^2\Psi_k/dQ_k{}^2+[8\pi^2\mu_k h^{-2}\Omega_k-4\pi^2\mu_k h^{-2}\Omega_k{}^2]\Psi_k=0, \quad (13)$$

where Ψ_k is a quasiwave function corresponding to the kth normal coordinate Q_k; μ_k denotes a reduced mass of the nuclei contributing to the kth vibration mode. It is obvious that the above equation solutions are basically determined by a model which is responsible for force-constant calculations, i.e., the second derivatives of a cluster potential with respect to given normal coordinates. An eigenenergy of the kth vibration mode is obtained as

$$\Omega_k(\nu_k)=2\Omega_{k0}(\nu_k+1/2), \quad (14)$$

where $\Omega_{k0}=(h/2\pi)(f_k/\mu_k)^{-1/2}/2$ is a zero-point motion energy and $\nu_k=0,1,2,\ldots$ is a vibration quantum number associated with the following quasiwave function:

$$\Psi_k(Q_k)=(2\Omega_0/\pi)^{1/4}(2^{\nu k}/\nu_k!)^{-1/2} \times\exp(-\Omega_{k0}Q_k{}^2)H_\nu((2\Omega_{k0})^{1/2}Q_k), \quad (15)$$

where $H_\nu(x)$ is a Hermit polynomial. The application of Eq. (15) is physically justified by an essential localization of the considered molecular fragment. Therefore, any change in the C_{60}-derivative clusters may be described as a local perturbation.

At the first stage, an electron-vibration interaction potential was calculated in a nonlinear approximation:

$$V_{e-v}(\mathbf{r}_i)=e^2\Sigma_{ms}M_{ms}{}^{-1/2}[Z_{ms}(\mathbf{r}_s-\mathbf{u}_{ms})|\mathbf{r}_s-\mathbf{u}_{ms}|^{-3} -\Sigma_{m's'}Z_{m's'}(\mathbf{r}_{s'}-\mathbf{u}_{m's'})|\mathbf{r}_{s'}-\mathbf{u}_{m's'}|^{-3}], \quad (16)$$

where M_{ms} and eZ_{ms} are the effective atomic mass and charge, for corresponding atoms numbered by m and s, respectively. The $\mathbf{u}_{ms,m's'}$ vector is a relative displacement of two atoms from their equilibrium positions $\mathbf{r}_s$ and $\mathbf{r}_{s'}$. The probability of optical transition induced by the vibration of a frequency Ω_k is equal to[25]

$$W^-(\Omega_k)=4(h/2\pi)^{-2}c^{-3}H^{-1}g^{-1}(\mathbf{r}_i)(\omega_{\rm el}-\Omega_k)^2B^-(\Omega_k), \quad (17)$$

where H is a sum of the η and ξ levels widths, $E_{\rm el}$ is an electron transition energy, Ω_k denotes a vibration energy, and $g(r_i)$ is a degeneration degree of the corresponding electron energy levels. The parameter $B^-(\Omega_k)$ is equal to[40]

$$B^-(\Omega_k)=\Sigma_\eta^{g(\eta)}\Sigma_\xi^{g(\xi)}|\{\Sigma_\varphi\langle\eta,\eta_\Omega|V_{e-v}(\mathbf{r}_i)|\varphi,\eta_{\Omega+1}\rangle\langle\varphi|\mathbf{d}|\xi\rangle \times(\omega_\xi-\omega_\eta+\Omega_k)^{-1}+\Sigma_\varphi\langle\eta|\mathbf{d}|\varphi\rangle \times\langle\varphi,\eta_\Omega|V_{e-v}(\mathbf{r}_i)|\xi,\eta_{\Omega-1}\rangle \times(\omega_\xi-\omega_\eta-\Omega_k)^{-1}\}|^2\overline{\theta}, \quad (18)$$

where η and the ξ are the lower and upper electron energy levels, respectively; φ denotes a virtual electron state, **d** is an electric dipole moment for a given spectral transition. The sums are performed over all degenerate initial and final states. $\overline{\theta}$ is the average of the occupation numbers of the vibration states with frequency Ω_k.

On the other hand, the symmetric vibrations included in the electron-vibration interaction [Eq. (18)] can be expressed in normal coordinates as

$$B^{-}(\Omega_k)=C_{\eta\xi}{}^{\gamma}(r_{\lambda}{}^{\Delta})C_{\eta\xi}{}^{\gamma'}(r_{\lambda'}{}^{\Delta'})\,\mathrm{Im}\,G_{\Delta\Delta'}{}^{\gamma\gamma'}(r_{\lambda}{}^{\Delta},\Omega_k{}^2), \tag{19}$$

where $G_{\Delta\Delta'}^{\gamma\gamma'}(r_{\lambda}^{\Delta})$ is a Green function (γ and γ' are numbers of the coordination sphere) defined as

$$G_{\Delta\Delta'}{}^{\gamma\gamma'}(r_{\lambda}{}^{\Delta})=\Sigma_{\varphi}\{\langle\eta|V_{e-v}(\mathbf{r}_i)|\varphi\rangle\langle\varphi|\mathbf{d}|\xi\rangle+\langle\eta|\mathbf{d}|\varphi\rangle \times\langle\varphi|V_{e-v}(\mathbf{r}_i)|\xi\rangle\}(\omega_{\xi}-\omega_{\eta})^{-1}. \tag{20}$$

We have performed the Green-function calculations for the C_{60} cycloadduct by performing the summations over 435 points in the irreducible part of the molecule. The resulting expression is given below:[38]

$$G_{\Delta\Delta'}{}^{\gamma\gamma'}(r_{\lambda}{}^{\Delta},\Omega_k{}^2) =\Sigma_{\Omega}K_{\Delta'}{}^{\gamma'}(r_{\lambda}{}^{\Delta})K_{\Delta}{}^{\gamma}(r_{\lambda}{}^{\Delta})(\Omega_k{}^2-\Omega^2-i\delta)^{-1}, \tag{21}$$

where the coordinates $K_{\Delta}^{\gamma}(r_{\lambda}^{\Delta})$ are obtained for a given vibration type from the electron states average. To include the molecular deformations into the Green function, we considered in our calculation the deformation localization that allows us to use the Dyson relations. The deformation potential and the corresponding charge defect determine the potential operator U and the corresponding Green functions:[42]

$$G_{\Delta\Delta'}{}^{\gamma\gamma'}(1)=G_{\Delta\Delta'}{}^{\gamma\gamma'}(0)+G_{\Delta\Delta'}{}^{\gamma\gamma'}(0)UG_{\Delta\Delta'}{}^{\gamma\gamma'}(1), \tag{22}$$

where $G_{\Delta\Delta'}{}^{\gamma\gamma'}(0)$ and $G_{\Delta\Delta'}{}^{\gamma\gamma'}(1)$ are the Green functions for the ideal and defected (by the vibrations) systems, respectively. We should point out that due to the complex aspect of the Green functions a relation between the real and imaginary parts may be obtained using Kramers-Kronig dispersion relations. These relations allowed us to extract the energy density of the electron-vibration states and to estimate their average lifetime $1/\eta$, the density $I(E)$ of the electron vibration states is given as

$$I(E)=\int (H/2\pi)W^{-}(\Omega_k)[(\omega-\omega_{\mathrm{el}}+\Omega_k)^2 +(\eta/2)^2]^{-1}d\Omega_k. \tag{23}$$

The consideration of the electron-vibration perturbation in calculations have essentially improved the agreement between the calculated results and the experimental data. The approximate molecular structure of the molecule together with the corresponding direction of the vibrations and electrostatic potential distribution optimized by means of the above method are presented in Fig. 7. We notice an asymmetry of the charge-density distribution due to the consideration of the intercluster fluctuation disturbance of the stationary electronic charge-density distribution (i.e., anharmonic electron-vibration interaction) and also an asymmetry of the CI vibration states. Such an asymmetry could essentially influence the optical properties of the C_{60}-1,3dithiole adduct and can cause a redistribution of averaging lifetimes between the levels determining these optical properties.

The calculated contribution of the vibration part is taken into account by a method previously described.[43] The linear environmental field (of the oligeotheracrylate matrices or of the benzene solutions) is presented as a linear frozen-core electrostatic potential system. Rotational functions of that state can be presented in the following form:[44]

$$R^{(J)}{}_{M\Omega}(\alpha,\beta,\gamma)=\exp(iM\alpha)[(2J+1)^{1/2}D^{(J)}{}_{M\Omega}(\beta) \times\exp(i\Omega\gamma)], \tag{24}$$

where angles α and γ involve only phase factors representing azimuthal rotations about the light polarization vector and the internuclear axis. In the case of unoriented molecules, the ground state is isotropic and all values of the angle β are equally available. The corresponding average using an integral procedure is performed using the standard methods of ground-excited-state interactions in the case of the EVR modes.

The appearance of the anisotropy in the longitudinal overlap integrals and transverse hopping integral is due to the laser pulse duration (several picosecond) which was shorter than the rotational relaxation time of the modified C_{60} molecule and to the applied external pressure, which decreased the distance between the considered atom and environmental atoms. To calculate the intermolecular interaction parameters, we introduced β-dependent orientational overlapping integrals:

$$IM=\int R^{(J)}{}_{M\Omega}(\alpha,\beta,\gamma)\psi^{*}{}_{\mathrm{env}}(r-r')d\beta'd^3r'. \tag{25}$$

A relation between the real and imaginary parts of the Green function may be obtained within the Kramers-Kronig dispersion relations.

The calculated dependences of the TPA with the inclusion of the vibration and rotational parts are presented in Fig. 8. In comparison with the calculated values and the experimental ones (see Fig. 2), we can consider the pressure-temperature modulation. Temperature influences first of all the vibrational part of the TPA, however, the hydrostatic pressure affects first of all the rotational part of the susceptibility. A consequence of the observed pressure dependences are contributions of the superposition of the vibrational and rotational parts to the measured nonlinear optical susceptibilities.

From Table I, we should note that inclusion of the electron-vibration interactions is important for the 2-thioxo-1,3-dithiole modified fullerenes. Simultaneously the experimental values of β are a little larger than the values predicted by the theoretical approach. This small difference can be caused by the solvent contribution.

VII. CONCLUSIONS

We have performed measurements of the TPA in a C_{60}-1,3dithiole cycloadduct as a function of temperature and

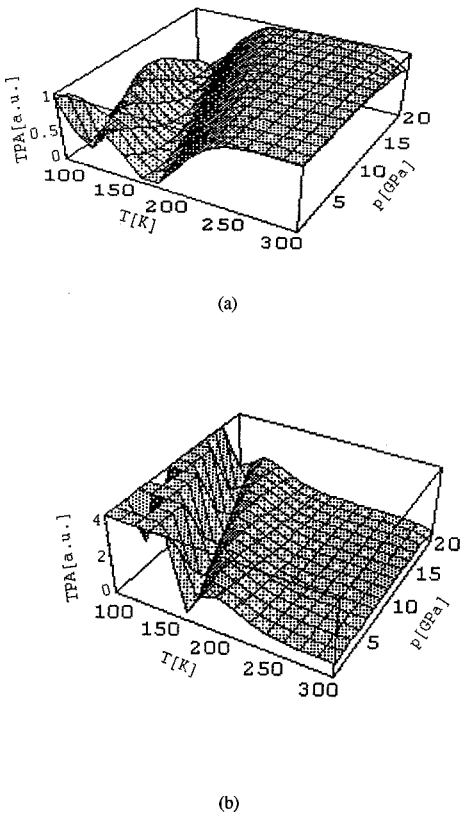

FIG. 8. Calculated final TPA pressure-temperature dependences with the inclusion of rotational and vibrational contributions for studied molecules, (a) C_{60}, (b) C_{60}-1,3-dithiole.

hydrostatic pressure. We revealed that below 230 K in the mentioned dependences there appear sharp maxima indicating the competition between the pressure-induced ordering and temperature disordering of the compounds.

Using the methods of the molecular-dynamics simulation and quantum chemical calculations, we found an asymmetry of the CI-electron-vibration states. Such an asymmetry essentially influences the optical properties of the C_{60} derivative and caused a charge-density redistribution both on the intramolecular as well as on the intermolecular level. Raman data allowed us to simplify taking into account the vibration states, restricting the choice of the pressure-dependent Raman modes. Directly on the border between C_{60} and the 1,3-dithiole moiety, we revealed an essential electronic charge-density redistribution and several asymmetries. Two types of Raman modes effectively contributing to the output TPA coefficients are revealed. The first type corresponds to the modes responsible for the intraplain vibrations and the second ones for the cycloadduct bond length.

We demonstrated an essential contribution of both the vibration and rotational subsystems to the observed pressure-temperature maxima of the TPA in the case of the cycloadduct of C_{60}. We estimate essential additional contributions of the dithiole core to the final nonlinear optical susceptibilities.

The observed sharp structure is a result of the competition between the temperature, which induces reorientation, and pressure, which stimulates the ordering of the investigated molecule. The Raman experiment can serve as confirmation of the essential role played by the vibration subsystem; it shows essential sensitivity to the external pressure and to the fact that the inclusion of the electron-vibration interactions is important for modified fullerenes. The Raman spectra show also that the influence of the solvents on nonlinear optical behaviors of the mentioned systems can be neglected. The theoretically calculated values of the β are slightly smaller then the measured values.

ACKNOWLEDGMENTS

The authors would like to thank Professor J. Zaremba for very helpful discussions and Professor M. D. Decotterd for his technical assistance. This work was supported by the Polish Committee for Scientific Research Grant No. KBN 2 PO3B 138 12.

*FAX: 33 2 41 73 53 30. Electronic address: sahraoui@babinet.univ-angers.fr

†Permanent adress: Institute of Physics WSP, Al. Armii Krajowej 13/15, 42201 Czestochowa, Poland.

[1] T. Cao and S. E. Weber, Macromolecules **28**, 3741 (1995).

[2] W. J. Blau, H. J. Byrne, D. J. Cardin, T. J. Dennis, J. P. Hare, H. W. Kroto, R. Taylor, and D. R. M. Walton, Phys. Rev. Lett. **67**, 1423 (1991).

[3] F. Kajzar, C. Taliani, R. Danieli, S. Rossini, and R. Zamboni, Chem. Phys. Lett. **217**, 418 (1994); Phys. Rev. Lett. **73**, 1617 (1994).

[4] A. Izuoka, T. Tashikawa, Y. Suzuki, M. Konno, Y. Saito, and J. Shinohara, J. Chem. Soc. Chem. Commun. **23**, 1472 (1992).

[5] A. Izuoka, T. Tashikawa, T. Sugawara, Y. Saito, and H. Shinohara, Chem. Lett. **34**, 1049 (1992).

[6] Z. Iqbal, R. H. Baughman, B. L. Ramakrishna, S. Khare, N. S. Murthy, H. J. Borneman, and D. E. Morris, Science **254**, 826 (1991).

[7] F. P. Strohkendl, L. R. Dalton, R. W. Hellwarth, H. W. Sarkas, and Z. Kafafi, J. Opt. Soc. Am. B **14**, 92 (1997).

[8] F. Kajzar, C. Taliani, R. Danieli, S. Rossini, and R. Zamboni, Synth. Met. **77**, 257 (1996).

[9] G. B. Alers, B. Golding, A. R. Kortan, R. C. Haddan, and F. A. Theil, Science **257**, 511 (1992).

[10] I. V. Kityk, B. Sahraoui, P. X. Hguyen, G. Rivoire, and J. Kasperczyk, Nonlinear Opt. **18**, 13 (1997).

[11] S. Mukamel, *Principles of Nonlinear Optical Spectroscopy* (Oxford, New York, 1995).

[12] A. J. McKellar, D. L. Yeager, J. A. Nichols, and J. T. Golab, J. Chem. Phys. **105**, 9927 (1996).

[13] T. N. Thomas, R. A. Taylor, J. F. Ryan, D. Mihailovic, and R. Zamboni, Europhys. Lett. **25**, 403 (1994).

[14] I. E. Kardash, V. S. Letokhov, Yu. E. Lozovik, Yu. A. Matveets, A. G. Steponov, and V. M. Farztdinov, Pis'ma Zh. Eksp. Teor. Fiz. **58**, 134 (1993) [JETP Lett. **58**, 138 (1993)].

[15] C. Boulle, M. Cariou, M. Bainville, A. Gorgues, P. Hudhomme, J. Orduna, and J. Garin, Tetrahedron Lett. **38**, 81 (1997).

[16] A. Hirsh, *The Chemistry of the Fullerenes* (Georg Thieme Verlag, Stuttgart, 1994).

[17] A. Hirsh, Synthesis **13**, 895 (1995).

[18] F. Diederich, and C. Thilgen, Science **271**, 317 (1996).

[19] I. V. Kityk, R. I. Mervinskii, J. Kasperczyk, and S. Jossi, Mater. Lett. **27**, 233 (1996).

[20] C. G. Broyden, J. Inst. Math. Appl. **6**, 222 (1970).

[21] R. Fletcher, Comput. J. (UK) **13**, 317 (1970).
[22] D. Goldfarb, Math. Comput. **24**, 23 (1970).
[23] D. F. Shanoo, Math. Comput. **24**, 647 (1970).
[24] D. P. Cgang and S. R. Langhoff, J. Chem. Phys. **84**, 5606 (1986).
[25] O. I. Shpotyuk, J. Kasperczyk, and I. V. Kityk, J. Non-Cryst. Solids **215**, 218 (1997).
[26] A. D. Becke, J. Chem. Phys. **98**, 1372 (1993).
[27] M. J. Frisch, G. W. Trucks, H. W. Schlegel, P. M. W. Gill, B. G. Johnson, M. W. Wong, J. B. Foresman, M. A. Robb, M. Head-Gordon, E. S. Replogle, R. Gomperts, J. L. Andres, K. Raghvachari, J. S. Binkley, C. Gonzales, R. L. Martin, D. J. Fox, D. J. Defrees, J. Baker, J. J. P. Steart, and J. A. Pople, GAUSSIAN 94, Rev. C3, Gaussian Inc., Pittsburg, 1994.
[28] D. E. Woon and T. H. Dunning, J. Chem. Phys. **98**, 1358 (1993).
[29] GAMES, General Atomic and Molecular Electronic Structure System, QCPE, 10, 52, 1990.
[30] J. A. Pople and D. L. Beveridge, *Approximate Molecular Orbital Theory* (McGraw-Hill, New York, 1970).
[31] I. V. Kityk, J. Kasperczyk, and B. V. Andrievskii, Phys. Lett. A **216**, 161 (1996).
[32] I. V. Kityk, Phys. Solid State **34**, 256 (1992).
[33] F. Rubinowitz, *Theory of the Molecular Vibration* (Bradley, Moscow, 1967), p. 125.
[34] G. B. Bachelet, D. R. Hamann, and M. Schluter, Phys. Rev. B **26**, 4199 (1982).
[35] J. B. Perdew and A. Zunger, Phys. Rev. B **23**, 5048 (1981).
[36] D. M. Ceperley and B. J. Alder, Phys. Rev. Lett. **45**, 566 (1980).
[37] D. J. Chadi and M. L. Cohen, Phys. Rev. B **8**, 5747 (1973).
[38] Ya. O. Dovgii, I. V. Kityk, and A. O. Matkovskii, Phys. Solid State **35**, 146 (1993).
[39] I. V. Kityk, J. Phys.: Condens. Matter **6**, 4199 (1994).
[40] O. T. Antonyak, I. V. Kityk, and N. S. Pidzyrailo, Opt. Spectrosc. **63**, 683 (1987).
[41] I. V. Kityk, B. Sahraoui, X. Nguyen Phu, G. Rivoire, and J. Kasperczyk, Nonlinear Opt. **18**, 13 (1997).
[42] I. V. Kityk, E. Jakubczyk, and Z. Mandecki, Mater. Sci. Eng., A **43**, 1045 (1997).
[43] E. Golis, I. V. Kityk, J. Wasylak, and J. Kasperczyk, Mater. Res. Bull. **31**, 1057 (1996).
[44] Ya. O. Dovgii and I. V. Kityk, *Band Energy Structure and Nonlinear Optical Susceptibilities of the Crystalline Solids* (Sweet, Lvov, 1996), p. 230.